Soft Matter

Characterizing the Spatiotemporal Evolution of Paramagnetic Colloids in Time-Varying Magnetic Fields with Minkowski Functionals

Journal:	*Soft Matter*
Manuscript ID	SM-ART-06-2020-001100.R1
Article Type:	Paper
Date Submitted by the Author:	03-Aug-2020
Complete List of Authors:	Hilou, Elaa; Rice University, Chemical & Biomolecular Engineering Joshi, Kedar; Rice University, Chemical and Biomolecular Biswal, Sibani; Rice University, Chemical & Biomolecular Engineering

Soft Matter

ARTICLE TYPE

Cite this: DOI: 00.0000/xxxxxxxxxx

Characterizing the Spatiotemporal Evolution of Paramagnetic Colloids in Time-Varying Magnetic Fields with Minkowski Functionals†

Elaa Hilou, Kedar Joshi, and Sibani Lisa Biswal*[a]

Received Date
Accepted Date

DOI: 00.0000/xxxxxxxxxx

Phase separation processes are widely utilized to assemble complex fluids into novel materials. These separation processes can be thermodynamically driven due to changes in concentration, pressure, or temperature. Phase separation can also be induced with external stimuli, such as magnetic fields, resulting in novel nonequilibrium systems. However, how external stimuli influence the transition pathways between phases has not been explored in detail. Here, we describe the phase separation dynamics of superparamagnetic colloids in time-varying magnetic fields. An initially homogeneous colloidal suspension can transition from a continuous colloidal phase with voids to discrete colloidal clusters, through a bicontinuous phase formed via spinodal decomposition. The type of transition depends on the particle concentration and magnitude of the applied magnetic field. The spatiotemporal evolution of the microstructure during the nucleation and growth period is quantified by analyzing the morphology using Minkowski functionals. The characteristic length of the colloidal systems was determined to correlate with system variables such as magnetic field strength, particle concentration, and time in a power-law scaling relationship. Understanding the interplay between particle concentration and applied magnetic field allows for better control of the phases observed in these magnetically tunable colloidal systems.

1 Introduction

One of the most active areas in colloid assemblies is the precise control of interparticle interactions. Field-directed colloidal-assemblies have a significant advantage over self-assembly processes in that the external field can modulate the assembly dynamics[1]. Dipolar colloids are typically characterized by induced directional interactions that result in head-to-tail ordering into clusters and chains[2]. Recent attention has focused on the use of rotating magnetic fields to generate colloids with a time-averaged dipolar potential[3–5]. Much research has focused on the generation of interesting equilibrium condensed phases of these systems, but the non-equilibrium dynamics of these dipolar systems are not well-characterized.

Investigating the non-equilibrium phase space of systems has demonstrated importance in the development of advanced materials[6–8]. However, most phase diagrams describe systems at their equilibrium or quasi-equilibrium states[9,10]. Quantifying the temporal changes of microstates is essential in achieving desired material properties[11]. Recently, it has been shown that the dynamics of binary systems such as emulsions[12], polymer mixtures[13,14], biological systems[15], and active fluids[16–20] exhibit novel processes. Complex morphology is associated with polymer mixtures assembling into lamella and gyroid phases, which can be explored using a tunable phase separating system[21,22]. Here, we investigate the pathways and transitions in a 2D colloidal system consisting of spherical superparamagnetic colloids in a time-varying magnetic field that resemble phase-separating systems[23]. The phase separation process usually consists of two mechanisms: rapid nucleation or decomposition of an initially homogeneous dispersion into domains of high and low densities, followed by the coarsening of these domains[24–26]. Additionally, from the two-phase region, phase inversion can occur via a complex connected spinodal phase.

The classic approach used to characterize the coarsening dynamics of most systems is to monitor the growth in the domain size over time, which has been shown via experiments and simulations to follow a power law behavior[21,27]. These dynamic scaling methods examine statistical measurements such as the structure factor and pair correlation functions[28,29]. What is missing is an understanding of how the connectivity of the system evolves as a function of the governing variables[16,30]. We correlate the nonequilibrium dynamics of our 2D dipolar fluid as a function of magnetic field strength and particle concentration to the characteristic lengths and quantify the changes in the microphase by utilizing Minkowski functionals, which identify changes in the area, A, boundary length, P, and the Euler characteristic, X, which indi-

[a]Department of Chemical and Biomolecular Engineering, Rice University, Houston, TX 77005, USA. E-mail: biswal@rice.edu; Tel: +1 713-348-6055.

† Electronic Supplementary Information (ESI) available: [The details of finding the threshold density as well as videos showing the dynamic phase separation]. See DOI: 10.1039/cXsm00000x/

cate the connectivity of the colloidal microphases over time. The equivalent functionals for a 3D system are area, volume, the Euler characteristic, and integral mean curvature. This methodology has been previously employed to characterize 2D polymer systems undergoing spinodal decomposition[30], which generally exhibit complex geometrical structures, but has not been applied to colloidal systems with discrete particles. This study evaluates the transitions between various microstates and presents scaling laws that correlate the dynamic length scale to magnetic field strength and particle concentration. The dynamical scaling coefficients are characteristic of a self-similar domain growth for colloids driven by time-varying magnetic fields.

2 Experimental

The experimental setup consists of paramagnetic particles dispersed in an aqueous solution and exposed to an external magnetic field. The cross-linked superparamagnetic polystyrene particles are $1.1 \pm 0.08\ \mu m$ in diameter and coated with a carboxylic acid group, making the surface negatively charged. They were acquired from ThermoFisher Scientific (Dynabeads® MyOne). The particles are diluted in a 10 mM NaCl solution at different densities ranging from 10 mg/ml to 0.67 mg/ml. The particle density is 1.8 g/cm^3, making it easy for them to settle to the bottom of the chamber. The chamber is composed of two plasma-cleaned cover slips (Ted Pella, Inc.) and a Paraffin film that is placed between the glass slips to act as a spacer and allow particles to flow in. The chamber is then sealed with epoxy followed by a layer of NOA 81 (Norland Optical Adhesive).

The magnetic field is generated by running a periodic current through two pairs of solenoids with a phase angle of 90 degrees resulting in a horizontally isotropic magnetic field[23]. Once the sample is placed between the four coils and a current is applied, the resulting rotational field produces an anharmonic interaction between the particles, which we can quantify theoretically and experimentally. A custom built inverted microscope is placed in the coil setup and used to image colloidal phase transitions. Time-lapse microscopy images are captured on a QICAM Fast camera with the software SimplePCI and a 4X magnification objective (Olympus Plan). This results in an image resolution of 0.44 pixels/μm. Image conversion and analysis were conducted using Matlab, using particle tracking packages[23].

3 Results and Discussion

3.1 Phase separating particles

Colloidal particles aggregate isotropically when placed in a high-frequency rotating magnetic field [see Fig.1(A)]. The variables that govern the resulting phases are the amplitude of the applied magnetic field, B, and the concentration of particles, ϕ, which is defined by the area fraction covered by particles. We have identified various microstates, which include voids, clusters, and a bicontinuous microphase, as shown in Fig.1(B). The ϕ range varied from 0.12 - 0.35. For a homogeneous colloidal system with high ϕ values, small gas pockets nucleate and ripen into larger voids within the colloidal matrix. At low ϕ values, the colloids nucleate into small clusters that coarsen over time. At intermediate ϕ values, the colloids form a labyrinth-like pattern. This pattern, characteristic of a bicontinuous phase, is metastable and appears during spinodal decomposition. This microstate may transition to isolated clusters, characteristic of a microstate observed at low ϕ values.

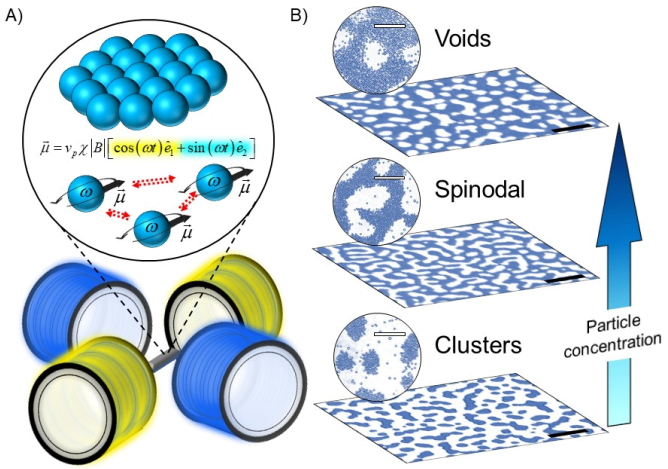

Fig. 1 Paramagnetic particles under the influence of a time-varying magnetic field. A) A schematic representing the setup of the coils used to drive the colloids to undergo phase transitions. B) Optical microscopy images of paramagnetic colloidal particles undergoing phase separation. Various microstates of interest are observed: clusters, spinodal, and voids. In these images, the particle concentration increases from the bottom to top image, while the applied magnetic field strength remains 9 Gauss. The black scale bar is 300 μm. The inset shows the particles under higher magnification. The white scale bar is 25 μm.

The pair interaction potential between these superparamagnetic colloids exhibits a long-range attractive interaction, described by $U_{pair}(r) \sim Ar^{-3}$, and a short-range Yukawa repulsion, which has similarities to the classic Lennard-Jones potential. Detailed description of this interaction can be found in our previous studies[23,31]. This potential energy is normalized by thermal energy, k_bT, which can be tuned by adjusting the magnitude of the magnetic field, as shown in Fig. 2(A). Recent simulations have provided a phase diagram for this system using colloids that varies the magnitude of the Yukawa repulsion[32]. We replot their results for hard-disks as a function of the minimum interparticle interaction energy, U_{min}, versus ϕ, and superimpose our experimental data, as shown in Fig.2(B). The critical point for their hard-disk model was determined to be $\phi = 0.32$. Our results compare well to their hard-disk model due to the short-range repulsion in our system. Note that our experimental limit for ϕ is 0.35, after which the system transitions from 2D to a multilayer 3D system.

The various phase separation pathways produce unique colloidal morphology's that depends on B and ϕ. Fig.2(C) shows a schematic illustrating four distinct pathways that are observed with this system. Clusters that coarsen over time can be observed in a system with low concentration relative to the critical point. As the concentration increases, the transition will pass through a bicontinuous phase, which can eventually break-up into clusters or maintain its bicontinuous structure within our time frame of

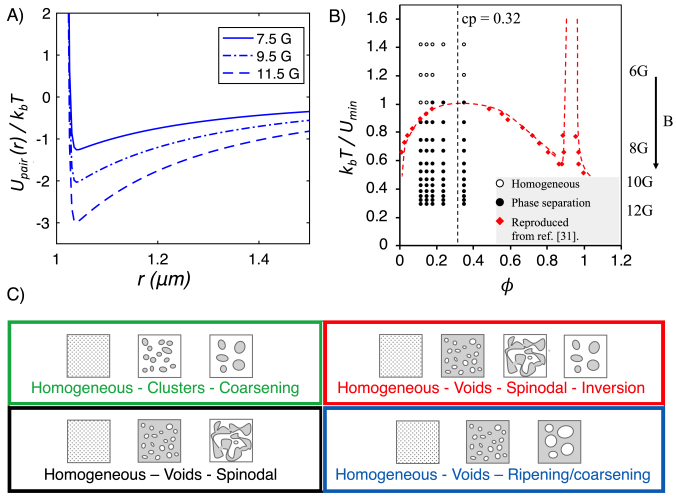

Fig. 2 Applying a high-frequency rotating magnetic field to a homogeneous dispersion of paramagnetic colloidal particles. A) The interaction potential energy (normalized by k_bT) between a particle pair due to long-range dipolar attraction and short-range Yukawa repulsion[23]. B) Experimental data points (in black) overlapping a phase diagram reproduced from ref.[32], showing that the transition between homogeneous to phase separated microstates depends on B and ϕ. C) A schematic of the various morphological pathways that can be experimentally observed in our system during phase separation. The four different colors represent the four different pathways that are further characterized in Fig.4 and Fig.5.

interest. Finally, a homogeneous system forms voids that coarsen over time at the highest concentration studied. In the following sections, we analyze the aforementioned structures using image processing techniques to visualize changes in the system morphology over time. We also show how the system transitions from one morphological state to another as it coarsens. In some cases, crossover occurs through all three states (voids, spinodal, and isolated clusters) before reaching a quasi-steady-state morphology within our experimental time frame.

3.2 Using Minkowski functionals to identify the morphological states

Minkowski functionals identify spatial patterns using integral geometry (described in detail in Ref.[30]). For example, in a dilute solution of monodispersed particles, the total boundary length, P, is the perimeter of a particle as observed experimentally, multiplied by the total number of particles present in that frame, while the total area, A, is the area of a single particle multiplied by the total number of particles. However, when using an objective with low magnification, the particles become indistinguishable from the background, especially at a high ϕ (see Fig.3(A)). Once the magnetic field is applied and the particles begin to aggregate, the system evolves from a single homogeneous gray domain to a combination of dark, colloid-rich domains and light colloid-poor domains, which represent areas with high and low particle concentrations, respectively. A detailed description of the threshold method used can be found in the supplementary information. As the system begins to phase-separate and well-defined domains become evident, the length of the interfacial boundary and the total area (in this case the area of the dark domains) can be determined. Due to coarsening, the measured colloid-rich area and its boundary will decrease over time and plateau, as shown in Fig.3(G) and Fig.3(H), respectively.

The Euler characteristic, X, is calculated by subtracting the number of voids from the number of clusters. A positive value of X corresponds to when clusters dominate the morphology in the sample, while a negative value indicates that the voids outnumber the clusters. The strength of the interaction between the particles, which is controlled via the applied time-varying magnetic field, governs the pathway of the phase separation. At higher magnetic fields, the system quickly forms a percolating colloidal network that segregates into colloidal-rich domains, which is why the values of A and P decrease as the magnetic field increases. Alternatively, a system can initially form voids that undergo an Ostwald ripening like process to form larger voids. Another observed transition is that a system initially consisting of voids undergoes phase inversion to eventually become a system of clusters.

At low magnetic field strengths, the dynamics of the phase transition becomes relatively slow. Previously, we demonstrated that at low magnetic field strengths, the magnitude of the line tension is on the order of thermal fluctuations[31]. Thermal fluctuations are thought to play a role in coarsening of binary fluids by driving coalescence[33,34]. This in turn, allows for a higher probability of capturing a system undergoing spinodal decomposition at low magnetic fields, where the line tension is small and comparable to thermal fluctuations. At low line tensions, the interface prefers to remain relatively flat, allowing the spinodal decomposition phase to exist as a quasi-equilibrium microstate.

3.3 Implementation of the Minkowski functionals

We use the Minkowski measurements to show the evolution in the morphological changes of a system under the same magnetic field but at different ϕ values. The dynamics are then analyzed from the initial field-on time until a quasi-equilibrium state is realized. Optical microscopy images of the nucleation to voids or clusters are depicted in Fig.4, which show how coarsening occurs over time at different ϕ values at a relatively low magnetic field of 7.5 Gauss. These particular experiments demonstrate the four specific pathways depicted in the schematic shown in Fig.2 (D). At this particular magnetic field and ϕ values of 35% and 20%, it is evident in Fig.4 that the system results in voids and clusters, respectively. However, the intermediate packing densities (28% and 22%) require a more quantitative measure of their morphological state. Using the Euler characteristic not only quantifies the connectivity, but also captures cases where phase inversion may occur. For example, a system might initially phase-separate into voids but form clusters later on as it coarsens.

We begin by examining the Euler characteristics of the packing densities mentioned and plotting them in Fig.5(A). At a high ϕ (35%), the particles condense rapidly to form many voids represented by the negative values of X, which then coarsen via a combination of Ostwald ripening and coalescence. The figure shows a rapid increase in the absolute value of X followed by a steady decrease over the span of 60 min. Within the same time frame

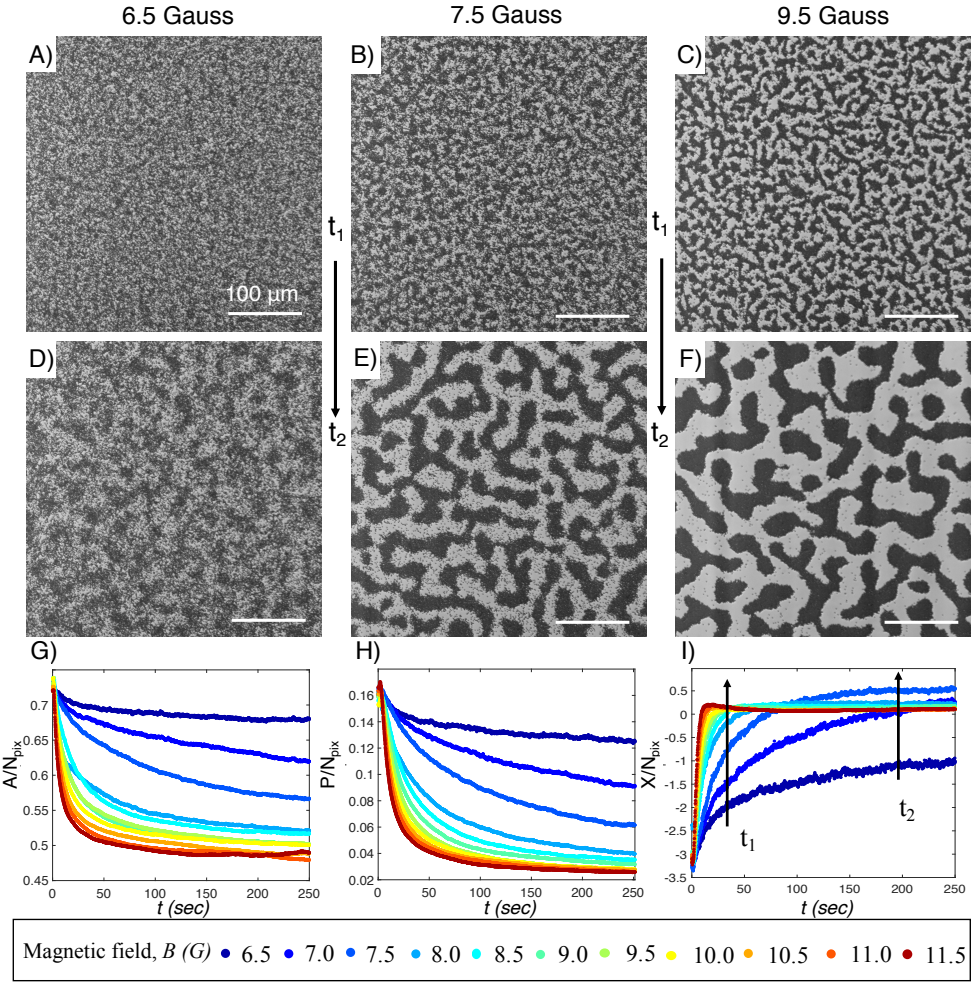

Fig. 3 Dynamics of Phase Separation (A) through (C) show initial snapshots of the paramagnetic particle system at 6.5 Gauss, 7.5 Gauss, and 9.5 Gauss, while (D) through (F) show the same samples undergoing phase separating into colloid-rich and colloid-poor regions at a later time. Scale bar 100 μm. (G) through (I) are plots of the three Minkowski functionals, A, P, and X, respectively as a function of time at different magnetic field strengths ranging from 6.5 Gauss (dark blue) to 11.5 Gauss (dark red). The values are normalized by the total number of pixels, N_{pix}, in an image.

and at a slightly lower concentration of 28%, the system begins to approach the spinodal regime and may qualitatively look like it has reached it; however, X is still negative, indicating the voids remain dominate. It is at 22% where the Euler characteristic crosses the zero mark soon after the external field is applied. At $\phi = 20\%$ the Euler characteristic begins with a positive X from early stage decomposition to the late stage as shown in the bottom left plot of Fig.5. This indicates a nucleation of many disconnected particles into clusters.

A physical interpretation of this phenomenon can be achieved by correlating P and X, which corresponds to the total curvature of the system. A system generally increases its curvature initially and then decreases that curvature over time. The increase is due to the formation of the domains with a total curvature of X/P as the system attempts to minimize its local energy; this is the main reason why decomposition occurs before coarsening. A decrease in the number of total domains as the system coarsens to reach its most energetically favorable state leads to a lower curvature over time as shown in Fig.5(B). However, this is generally the case for clusters and voids because they tend to have higher curvatures until the system enters the spinodal regime. In the case of $\phi \sim 28\%$, where the system is approaching a spinodal phase but is not quite there, the system exhibits a faster decrease of curvature that plateaus within the same time frame compared to ϕ=35% and ϕ=20%. A more complex case would be a suspension with a packing density of 22%, where clusters begin to form soon after the aggregation passes through the spinodal regime, but unlike ϕ=20%, X plateaus at a positive value close to zero, while P continues to decrease, leading to a slight increase in curvature over time. This is because the percolating network is easily disrupted, forming clusters that tend to coalesce with neighboring domains, thereby reducing interfacial length.

3.4 Length scale correlation

The dimensions of the colloidal features can be obtained by taking a Fast Fourier Transform (FFT) of the microscopy images. We measure the characteristic length scale, L, by finding the wavenumber, k, from the peak of the FFT radial average. The wave vector is inversely correlated to the length scale as $k = 2\pi/L$. Previous research[21,35,36] has shown that the characteristic length

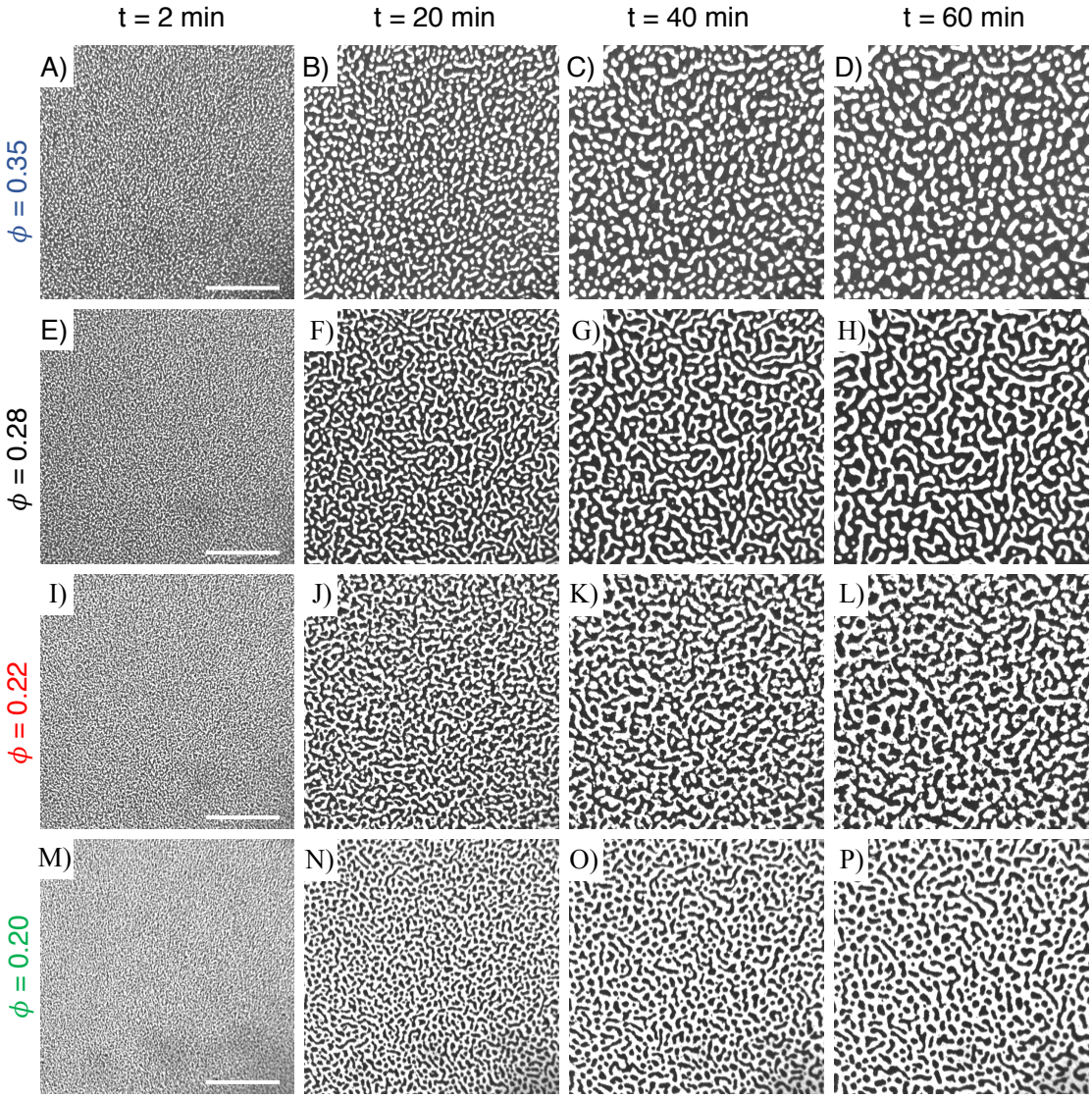

Fig. 4 Optical microscopy images of the time evolution of paramagnetic particles undergoing phase separation at various densities. Snapshots are taken after 2 min, 20 min, 40 min, and 60 minutes of applying the field. B = 7.5 Gauss. Scale bar 500 μm.

scale in the aggregation of dipolar systems typically exhbit a power law dependence with time, $L \sim t^m$. The value of m depends on the interactions and dimensions of the system. We aim to find a more comprehensive equation for L that will account for both the magnetic field and concentration of the system, $L = f\{t, B, \phi\}$. The Hamiltonian of such systems is homogeneous, so we assume that all parameters t, B, and ϕ are not strongly interdependent and for the most part, we can write $L = f_t(t) f_B(B) f_\phi(\phi)$. This separation of variables works well for slowly driven systems, which is true for weak magnetic fields. However, at strong fields (where $U_{pair} >> k_b T$) and higher concentrations, this assumption may not hold true. We analyze L as a function of time for different fields and concentrations. The data can be scaled to t^m, where $m = 0.35 - 0.4$ (see Fig.6(A)). The m values are shown by the inset plot for varying fields and concentrations. This has been shown previously for 2-D structures[35]; thus, $f_t(t) \sim t^{0.4}$. To understand the relationship between the length scale and magnetic field, we conducted experiments at different magnetic fields strengths while keeping the particle concentration fixed. The experiments were performed on the same sample by allowing the system to redisperse uniformly after each experiment. When considering the energy of the system under a rotating magnetic field, the length scale ($\sim \sqrt{size}$) is expected to evolve proportionally to the strength of the magnetic field, B, assuming an isotropic distribution. We performed the experiments at different magnetic fields and scaled L with $t^{0.4}$. The value of $Lt^{0.4}$ exhibits a linear relationship with B as shown in Fig.6 (B) for different values of ϕ. Thus, $f_t(t) = B$. Unlike the magnetic field, L is not a trivial function of the particle concentration. For a higher magnetic field, the line tension is greater and thus the system quickly adopts a cluster or void dominant morphology, followed by coarsening. Cluster and void growth follow the aggregation kinetics shown in previous studies[36]. On the other hand, for a lower magnetic field (lower line tension), the system goes from a homogeneous system to a

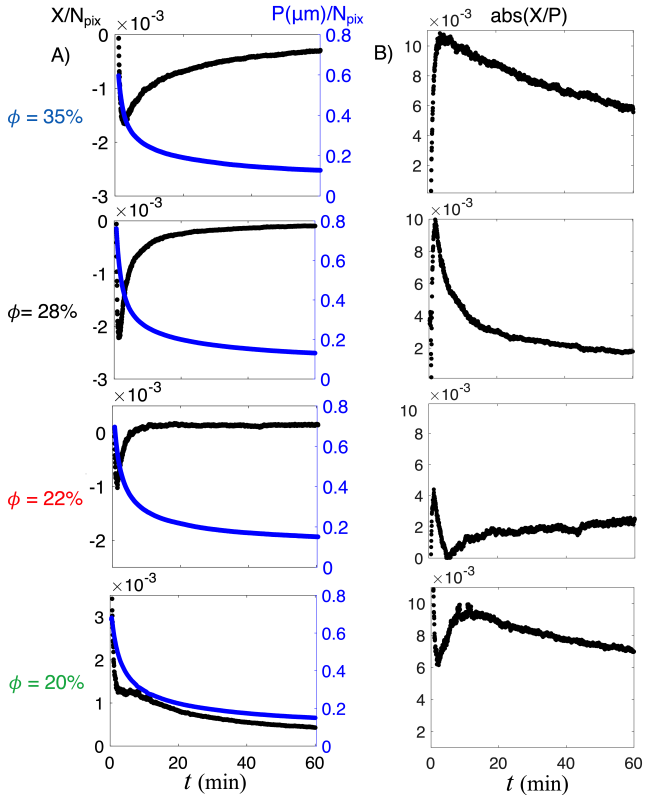

Fig. 5 Effect of particle density on the Minkowski measurements at B = 7.5 Gauss. (A) The Euler characteristic and boundary length as a function of time. (B) The absolute value of Euler over boundary length; which represents the curvature in 2D. Note how the "curvature" decreases over time to reach a more energetically favorable boundary, but in the case of ϕ = 22%, the system goes through a curvature of zero after approximately 5 min, implying that the system passes through a spinodal structure that coarsens and then breaks up into clusters.

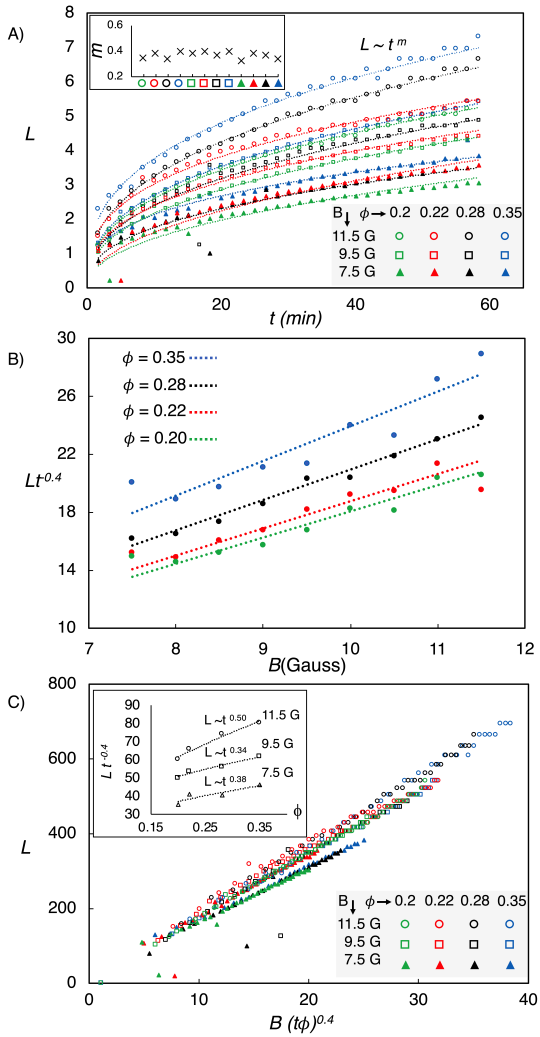

Fig. 6 Length scale correlation with system parameters: time, field, and concentration. A) Power law relation between length scale and time, which corresponds to $L \sim t^{0.4}$. Inset shows the value of m for each data set. B) Linear proportionality between the scaled length scale and magnetic field. C) Master plot that incorporates all conditions that will help predict L as a function of t at any B and ϕ. Inset shows the power law dependence on concentration.

spinodal state, which then coarsens into clusters over time. The low magnetic field strength allows for a slightly longer time for a system to remain in a meta-stable state, since the rearrangement is driven by the energy of the interface. We performed experiments with varying particle concentrations while keeping the field strength constant. Trends are shown in the internal figure in Fig. 6 (C). A typical aggregation kinetics for a 2D system[35] shows a $\phi^{0.4}$ dependency on the length scale dynamics. This assumes a uniform size and growth rate. The power observed is different for each field and averages approximately to 0.4, which we have used to propose a time-evolving equation for understanding the length scale dynamics: $l = cB(\phi t)^{0.4}$. Here, c is a constant that mainly depends on the properties of the suspending fluid. Fig. 6 (C) shows L vs. $B(\phi t)^{0.4}$ for different concentrations and magnetic fields. The data follow a linear trend. The expected L values at a lower magnetic field (approximately 7.5G) are slightly lower, as discussed above. The results from the Minkowski functionals, combined with the length scale of the system, are shown in Fig.7. The average length scale is the equivalent of the total perimeter divided by the Euler characteristic[30]. The more regular the shapes are, such as voids and clusters, the better this assumption applies. For a homogeneous system (clusters or voids), $[P/X]$ and L are correlated. Here, the morphology results in highly curved interfaces. Thus, the value of $[P/X]/L$ remains constant over a coarsening process. This is clearly observed in Fig. 7 (ϕ = 35% voids and ϕ= 20% cluster). For ϕ= 28%, the overall perimeter is slowly increasing, keeping X and L constant. Since the overall structure is voids (X<0), and the $[P/X]/L$ remains negative. Given additional time, the system may have undergone spinodal decomposition. For $\phi = 22\%$, the system passes through the spinodal regime and changes the sign of X. This transition is distinctly reflected in $[P/X]/L$. Lastly, for ϕ= 20%, the spinodal decomposition occurs very quickly and then the $[P/X]/L$ settles to a constant positive value, resulting in clusters. This analysis shows a simple and efficient method for detecting the spinodal regime and understanding the near spinodal dynamics by combining the length scale and Minkowski parameters in active fluids.

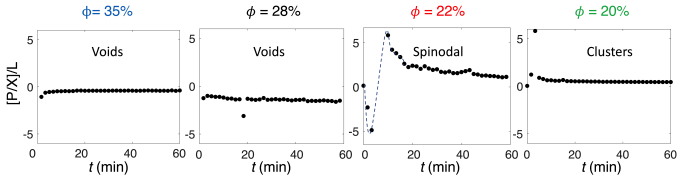

Fig. 7 Correlation between Minkowski functionals and the length scale of the system. Note that this correlation can identify the time at which phase inversion occurs. $B = 7.5$ Gauss

4 Conclusion

In summary, we implement the Minkowski functionals on a system of paramagnetic particles under a rotational magnetic field. We demonstrate how correlating the Minkowski parameters with the length scale of the system will result in a much more cohesive representation of phase separation dynamics. Under different conditions, such as particle concentration and field strength, the system will experience different phase separation pathways. We capture the morphological states of a system and explore the dynamics and how they coarsen over time. This was achieved by plotting the time evolution of the Minkowski parameters, curvature, and the characteristic length scale over time. Whether this can be used as a model system to study the phase separation of confined polymers and lipid bilayers, or for its wide range of applicability in other 2D materials, a better understanding of the phase transitions and the associated scaling dynamics can be used to control active fluid systems.

Conflicts of interest

There are no conflicts to declare.

Acknowledgments

This work was funded by the National Science Foundation under Grant No. CBET-17055703 and the National Science Foundation Graduate Research Fellowship under Grant No. 1450681.

Notes and references

1 V. Liljeström, C. Chen, P. Dommersnes, J. O. Fossum and A. H. Gröschel, *Curr. Opin. Colloid Interface Sci.*, 2019, **40**, 25–41.
2 S. H. Klapp, *Curr. Opin. Colloid Interface Sci.*, 2016, **21**, 76–85.
3 S. Jaeger, H. Schmidle and S. H. Klapp, *Phys. Rev. E*, 2012, **86**, 011402.
4 A. T. Pham, R. Seto, J. Schönke, D. Y. Joh, A. Chilkoti, E. Fried and B. B. Yellen, *Soft matter*, 2016, **12**, 7735–7746.
5 A. Weddemann, F. Wittbracht, B. Eickenberg and A. Hutten, *Langmuir*, 2010, **26**, 19225–19229.
6 T. Heuser, R. Merindol, S. Loescher, A. Klaus and A. Walther, *Advanced Materials*, 2017, **29**, 1606842.
7 W.-G. Lim, C. Jo, A. Cho, J. Hwang, S. Kim, J. W. Han and J. Lee, *Adv. Mater.*, 2019, **31**, 1806547.
8 C. G. Sztrum and E. Rabani, *Advanced Materials*, 2006, **18**, 565–571.
9 I. Ohnuma and K. Ishida, *Tecnologia em Metalurgia, Materiais e Mineracao*, 2016, **13**, 46.
10 M. A. Miller and D. Frenkel, *J. Chem. Phys.*, 2004, **121**, 535–545.
11 H. Chang, W. Yook, E. Park, J. Kyeong and D. Kim, *Acta Mater.*, 2010, **58**, 2483–2491.
12 R. Shimizu and H. Tanaka, *Nat. Commun.*, 2015, **6**, 7407.
13 P.-G. de Gennes, *J. Chem. Phys.*, 1980, **72**, 4756–4763.
14 J. Sabin, A. E. Bailey and B. J. Frisken, *Soft matter*, 2016, **12**, 5325–5333.
15 C. F. Lee and J. D. Wurtz, *J. Phys. D*, 2018, **52**, 023001.
16 M. Han, J. Yan, S. Granick and E. Luijten, *Proc. Natl. Acad. Sci.*, 2017, **114**, 7513–7518.
17 R. Alert, P. Tierno and J. Casademunt, *Proc. Natl. Acad. Sci.*, 2017, **114**, 12906–12909.
18 Q. Liu, P. J. Ackerman, T. C. Lubensky and I. I. Smalyukh, *Proc. Natl. Acad. Sci.*, 2016, **113**, 10479–10484.
19 G. S. Redner, M. F. Hagan and A. Baskaran, *Phys. Rev. Lett.*, 2013, **110**, 055701.
20 N. H. Nguyen, D. Klotsa, M. Engel and S. C. Glotzer, *Phys. Rev. Lett.*, 2014, **112**, 075701.
21 A. T. Pham, Y. Zhuang, P. Detwiler, J. E. Socolar, P. Charbonneau and B. B. Yellen, *Phys. Rev. E*, 2017, **95**, 052607.
22 N. Debnath, T. Kawaguchi, H. Das, S. Suzuki, W. Kumasaka, N. Sakamoto, K. Shinozaki, H. Suzuki and N. Wakiya, *Sci. Technol. Adv. Mater.*, 2018, **19**, 507–516.
23 D. Du, D. Li, M. Thakur and S. L. Biswal, *Soft Matter*, 2013, **9**, 6867–6875.
24 K. Jørgensen and O. G. Mouritsen, *Biophys. J.*, 1995, **69**, 942–954.
25 T. Petersen, M. Z. Bazant, R. J. Pellenq and F.-J. Ulm, *Phys. Rev. Mat.*, 2018, **2**, 095602.
26 R. Alert, P. Tierno and J. Casademunt, *Nat. commun.*, 2016, **7**, 13067.
27 H. Snyder and P. Meakin, *J. Chem. Phys.*, 1983, **79**, 5588–5594.
28 Y. Gao, J. Kim and M. E. Helgeson, *Soft Matter*, 2015, **11**, 6360–6370.
29 H. D. Vuijk, J. M. Brader and A. Sharma, *Soft matter*, 2019, **15**, 1319–1326.
30 K. R. Mecke, *Statistical Physics and Spatial Statistics*, Springer, 2000, pp. 111–184.
31 E. Hilou, D. Du, S. Kuei and S. L. Biswal, *Phys. Rev. Mater.*, 2018, **2**, 025602.
32 N. P. Kryuchkov, F. Smallenburg, A. V. Ivlev, S. O. Yurchenko and H. Löwen, *J. Chem. Phys.*, 2019, **150**, 104903.
33 C. del Junco, L. Tociu and S. Vaikuntanathan, *Proc. Natl. Acad. Sci.*, 2018, **115**, 3569–3574.
34 F. J. Alexander, S. Chen and D. W. Grunau, *Phys. Rev. B*, 1993, **48**, 634.
35 H. See and M. Doi, *J. Phys. Soc. Jpn.*, 1991, **60**, 2778–2782.
36 J. H. Promislow, A. P. Gast and M. Fermigier, *J. Chem. Phys.*, 1995, **102**, 5492–5498.

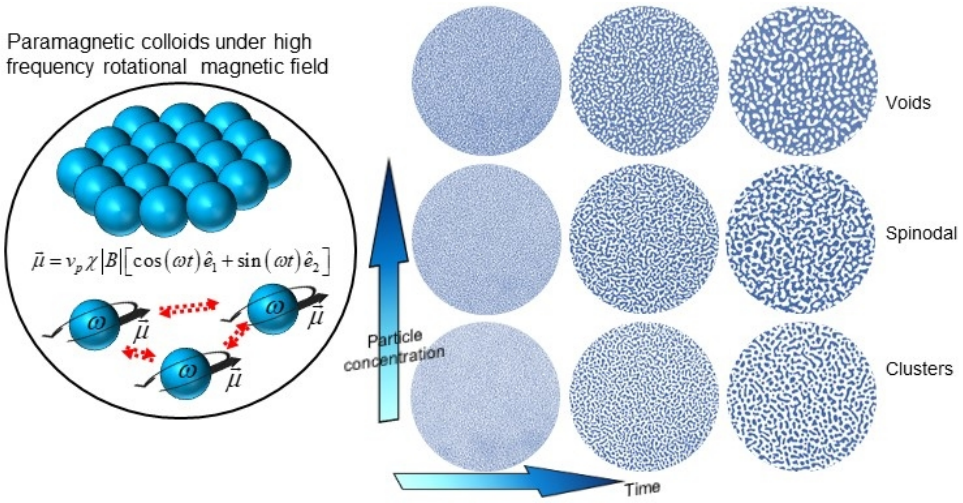

203x101mm (96 x 96 DPI)